

## EXPERIMENTAL AND NUMERICAL ASSESSMENT OF FRP STIRRUPS DISTANCE ON CYCLIC BEHAVIOR OF RC JOINTS\*

M. K. SHARBATDAR, \*\* A. DALVAND AND A. HAMZE-NEJADI

Faculty of Civil Engineering, Semnan University, Semnan, I. R. of Iran, Postal Code: 3513119111  
Email: msharbatdar@semnan.ac.ir

**Abstract**– Many reinforced concrete structures are exposed to corrosive environment which can lead to damage of the reinforcing steels. These members include coastal structures subjected to wind-born salt spray and seawater, as well as bridges beams and decks subjected to deicing salt. Design engineers should prevent the deterioration of reinforcing steel, especially transverse stirrups. Using FRP materials in new concrete members has attracted researchers' interests due to FRP high resistance against corrosion. Distance of FRP stirrups plays a key role in the cyclic behavior of joints and energy absorption magnitude. In this study, experimental and finite element investigations have been studied to assess the effects of stirrup distances on the cyclic behavior of concrete joints. In the experimental study, two half-scale concrete joints with the same beam and column dimensions and longitudinal steel reinforcing characteristics but different distance of transverse FRP stirrups were tested under cyclic loading. Besides presenting and analyzing the main results and photographs of the experimental tests, the made ANSYS finite element models were compared and validated with these tests. Moreover, the distances of FRP stirrups were varied in finite element models. According to experimental and finite element method results, the joints with congested stirrups had not only higher ductility and energy dissipation, but also had additional capacity, as much as 12% relative to the non-ductile joint with wider distance stirrups.

**Keywords**– Concrete joint, FRP stirrup, finite element method, ductility, cyclic behavior, experimental results

### 1. INTRODUCTION

Steel reinforcing bars are vulnerable to oxidation when exposed to chlorides. Examples of such exposure include marine areas and regions where road salts are used for deicing and also the locations where salt contaminated aggregates are used in the concrete mixture. Application of FRP bars in the form of longitudinal bars and stirrup in bridges, slabs and buildings is increasing as a result of their high resistance to corrosive regions [1-3]. The use of FRP composites in strengthening members of reinforced concrete structures such as beams and joints has been of great interest for civil engineers in recent years [4-6]. Various design codes for using FRP material in concrete structures were presented [7-10]. Many existing reinforced concrete buildings were already designed for gravity loads and lateral forces that may be much smaller than those prescribed by existing building codes [11]. Berg and others have studied cost analysis of an FRP reinforced concrete bridge deck. Their conclusions showed that construction of an FRP reinforced concrete bridge deck using conventional construction technology and labor was accomplished with a 57% savings in construction labor over nominally identical steel rebar reinforced deck [12]. Many researchers such as Nanni et al. have studied FRP reinforcement in concrete and assessed tensile properties of braided FRP rods for concrete reinforcement [13]. Li et al. studied reinforcement of concrete beam-column connections with hybrid FRP sheet [14]. Gadve et al. have conducted an experimental work on corrosion of steel reinforcements embedded in FRP wrapped concrete [15]. Lau and his colleagues

---

\*Received by the editors May 2, 2012; Accepted May 26, 2013.

\*\*Corresponding author

analyzed the experimental behavior of hybrid FRP reinforced concrete beams [16]. Gravina and Smith assessed the flexural behavior of indeterminate concrete beams reinforced with FRP bars [17]. Longitudinal bars had the greater diameter relative to stirrups and were far from corrosive environment. Therefore, effect of corrosion on longitudinal reinforcement was much less than stirrups. Performance of stirrups was very effective for cyclic behavior of members and flexibility and energy absorption capacity. Stirrup corrosion reduces the capacity of members and performance of structure in seismic loads. Seismic design code of steel RC frames was provided as ACI-318, giving some regulations regarding concrete structures ductility corresponding to the use of steel stirrups [18].

There has been no considerable research about cyclic behavior of concrete structures having man-made in-placed fabricated FRP transverse stirrups. One of the problems in using factory pre-fabricated grid stirrups is the unavailability of FRP grids and cost inefficiency in small projects. Man-made in-place stirrups introduced in this experimental study compared to fabricated types are easily assembled and compatible with any arrangement of longitudinal reinforcements such as triangular, rectangular and circular types. This study is mainly concentrated on the performance of the new proposed FRP stirrups in concrete joints with steel longitudinal reinforcement. Therefore, two concrete joints including different spacing FRP stirrups and constant steel longitudinal reinforcements were constructed and tested under the cyclic loading. The FRP stirrups distance in the specific critical region of beam and column was 50mm in the first joint while this space was 100mm in the other. Moment-drift, moment-curvature and moment-strain diagrams for FRP stirrup were achieved. Finally, FEM model was validated by experimental results and four more numerical models were constructed. So there were two groups of FEM models, two joints in each group. The first joint utilized closed space FRP stirrups and the latter used wider spacing stirrups with expected less ductility. Based on the results obtained from FEM analysis, the load-deformation curves and ductility coefficient of joints were calculated.

**2. EXPERIMENTAL RC JOINTS SPECIMENS**

In order to examine the effect of FRP stirrups distance on the cyclic behavior of concrete joints, two half-scale specimens were constructed with the same steel longitudinal bars (8 $\phi$ 14 in columns and totally 6 $\phi$ 12 at the top and bottom of the beams) and same dimensions, 250 mm square columns and 200 by 250 mm beams (height by width). The first joint had closed space FRP stirrups considering design code ductility regulations and was introduced as FDJ (FRP Ductile Joints), and the other had wider double spaced FRP stirrups and was introduced as FNJ (FRP Non-ductile Joints). Characteristics of the joints have been shown in Fig.1 and given in Table 1.

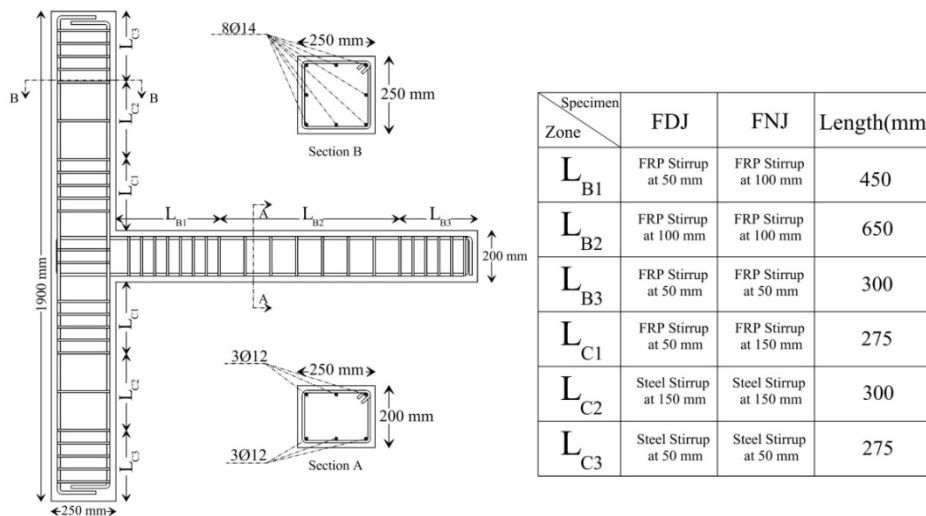


Fig. 1. Schematic of joint specimens

Table. 1. Details of experimental joint specimens with CFRP materials

Specimen	Number of rods (14 mm)	Number of rods (12 mm)		Stirrups Distance in the ductile region (mm)		Stirrups Distance in the non-ductile region (mm)		Number of stirrups in joint
		bottom	top	Beam	Column	Beam	Column	
FDJ	8	3	3	50	50	100	150	2
FNJ	8	3	3	100	100	100	150	1

**a) Material properties**

Seven and 28-day compressive strengths of concrete cylinders used in the joints were 21 and 30 MPa, respectively. Maximum aggregate size and slump of the used concrete were 10 and 80 mm, respectively. Yield and ultimate strength of steel longitudinal bars of column were 408 and 470 MPa. Furthermore, yield and ultimate strength for steel longitudinal rods of beams were 354 and 542 MPa. CFRP sheet texture was used to fabricate man-made in-place FRP stirrups for our experimental specimens. FRP stirrups cross section shown in Fig. 2 for the joint specimens was 7.8 mm<sup>2</sup>. Mechanical properties of fibers provided by manufacturer are given in Table 2. These fibers were initially sheets which, upon consideration of cross section thickness equal to 0.11 mm, were cut as strips. Cut strips were treated and completely covered by resin and were installed as stirrups in determined places on the steel longitudinal bars.



(a) Original FRP sheet                      (b) Cutting FRP strips                      (c) Stirrups installed in joints

Fig. 2. Used FRP fibers for In-placed Stirrups

Table 2. Mechanical properties of CFRP fibers

Product	Fiber Type	Tensile strength (MPa)	Modulus of Elasticity (GPa)	Ultimate strain (%)	Thickness per fiber (mm)
YC-N200	High Resistance Carbon	3550	235	1.5	0.11

**b) FRP stirrups design**

To design the FRP stirrups cross section, equivalent cross section of steel stirrup was adopted by assuming 6mm diameter steel stirrups, 28.3 mm<sup>2</sup> cross section and 260 MPa yield strength. According to design code regulations of ACI 318, shear capacity of steel stirrups was calculated by Eq. 1 [18].

$$V_s = \frac{A_{sv} F_y d}{S_s} \tag{1}$$

where  $A_{sv}$ ,  $F_y$ ,  $d$  and  $S_s$  are the sum area of two steel stirrups legs, steel bar yield strength, effective height and spacing of steel stirrups, respectively. If FRP fibers are used, shear capacity of FRP stirrups is calculated by Eq. 2 based on ACI 440 and Canadian design code CSA [8, 9].

$$V_f = \frac{A_{fv} f_{fv} d}{s} \tag{2}$$

where  $V_f$ ,  $A_{fv}$ ,  $s$ , and  $f_{fv}$  are shear capacity of FRP stirrups, sum area of two FRP stirrups legs, spacing of stirrups, and effective tensile strength of FRP stirrups.

According to ACI-440-R1, effective tensile strength in FRP stirrups is assumed to be  $0.004E_f$  when  $E_f$  is the modulus of elasticity of FRP stirrups. Required equivalent cross section of FRP stirrups was calculated according to Eq. 3 by assuming 0.4% strain for FRP stirrups and equality of shear capacity of FRP and steel stirrups. These results are presented in Table 3.

$$A_f = \frac{A_{sv} F_y}{0.004 E_f} \quad (3)$$

Table 3. Equivalent area of FRP stirrups

Cross section of a stirrup (mm <sup>2</sup> )		Yield strength of equivalent steel stirrups (MPa)	Modulus of elasticity of FRP fibres (GPa)
Equivalent steel stirrup	FRP stirrup	260	235
28.3	7.8		

### c) Experimental test set-up

Experimental set-up has been shown in Fig. 3, using two jacks set horizontally at the top of each specimen to apply cyclic load at the tip of the beam and one jack set at the end of the column to apply the axial loading to column. The other end of column was fixed to joint support. The applied constant axial load of 350 kN was equal to 20% of maximum nominal compressive capacity of the column and calculated from Eq. (4).

$$P_n = 0.85 f'_c (A_g - A_s) + A_s f_y \quad (4)$$

According to Fig. 4, applied horizontal loading was initiated as displacement cyclic control with 3 cycles in 0.5% drift with displacement equal to 6.25 mm. Next loading stages were comprised of three cycles per incremental loading stage. To determine the beam tip displacement and total beam-column joint rotation, two LVDTs were used at the top of the beam, as well as two more diagonal LVDTs at the beam-column intersection. All instrumentation tools were plugged into the information Data Logger machine to record all test data.

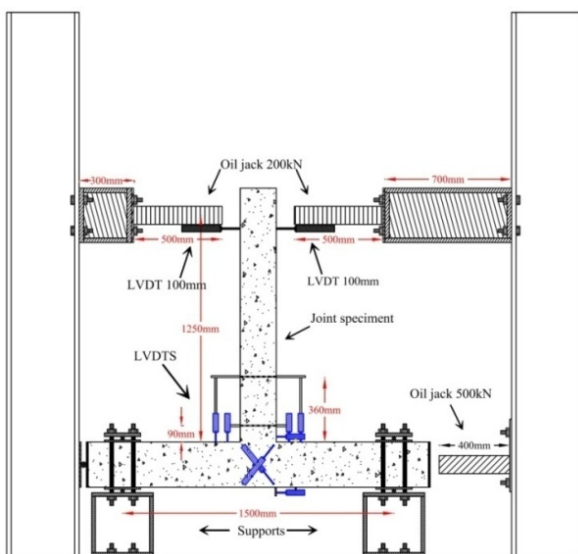


Fig. 3. Details of test set-up

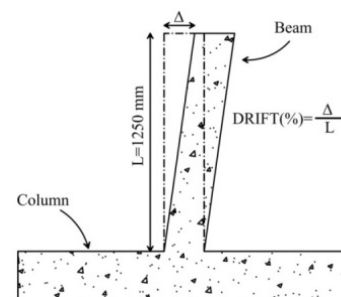


Fig. 4. Relative displacement of the beam with respect to joint column

### 3. CYCLIC PERFORMANCE OF EXPERIMENTAL JOINT SPECIMENS

The weak beam-strong column idea was expected in both specimens to have relative ductile joints. Fig. 5 shows Moment-Drift diagrams in both experimental specimens. These diagrams illustrate the stable behavior of joints up to 7% drift. Cracks were widened and this was the case for previous cracks as well in drifts 2-7%. Finally, diagonal shear crack occurred in the beam and near the joint. Moreover, cracks development and depth increasing continued in the joint region, and this was repeated up to the end of loading upon achieving 7% drift. Joint specimens at the end of tests with close-up details of crack patterns of two specimens are illustrated in Fig. 6.

Ductile specimen FDJ had the highest loading capacity as much as 12% higher than non-ductile specimen FNJ. In FDJ specimen, initial yield in steel longitudinal bars occurred in the moment and displacement of 15.16 kN.m and 0.89 mm, respectively and 18.91 kN.m and 12.44 mm at FNJ specimen. FDJ experienced longitudinal bars yielding in the smaller displacement, 20% lower compared to FNJ. Ductility of specimens based on the ratio of ultimate displacement to yielding displacement ( $\Delta_u/\Delta_y$ ) or the ratio of ultimate drift to yielding drift in FDJ and FNJ were 8.6 and 6.8, respectively, therefore closed spacing stirrup specimens showed 25% higher ductility compared to the wide spacing stirrup non-ductile specimen, indicating the FRP stirrups positive effects on the cyclic performance of RC joints reinforced with non-metallic stirrups. Steel RC joint specimen with the same characteristics and steel longitudinal and stirrups was tested under cyclic loading and showed stable behavior up to 7% with the ductility coefficient equal 7.5[19]. The comparison of steel and FRP stirrup joint specimen showed that both had almost the same ductility behavior, even more at the FRP specimen, indicating that the proposed designed and tested specimen had the ductility criteria the same as the steel stirrup specimen joint.

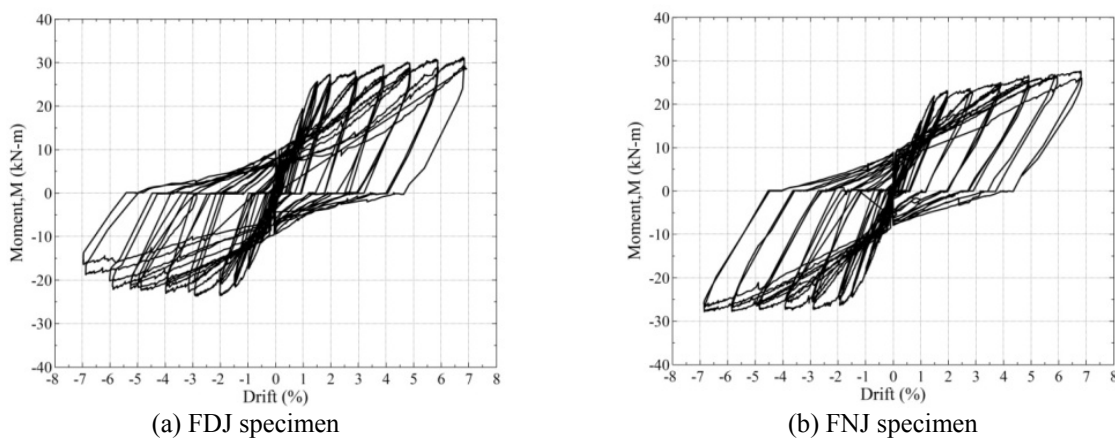


Fig. 5. Moment-displacement diagram of the joints

Moment-drift back-bone curves of the joints have been shown in Fig. 7. The slope of this specimen was very steep up to 1.5% and then decreased from 1.5% to 7% and no capacity degradation was observed up to the end of loading. Table 4 presents the maximum values of the positive and negative moments for both specimens. FNJ has the maximum positive moment which is 11.5% lower than FDJ. FNJ has the maximum negative moment which is 17.2% higher than FDJ.

Table 4. Maximum positive and negative moments in specimens

Specimen	$P^+_{max}$ (kN)	$P^-_{max}$ (kN)	Decreasing with respect to reference specimen (FDJ)	
			$P^+_{max}$ (%)	$P^-_{max}$ (%)
FDJ	31.25	23.75	---	---
FNJ	27.66	27.84	11.5	17.2

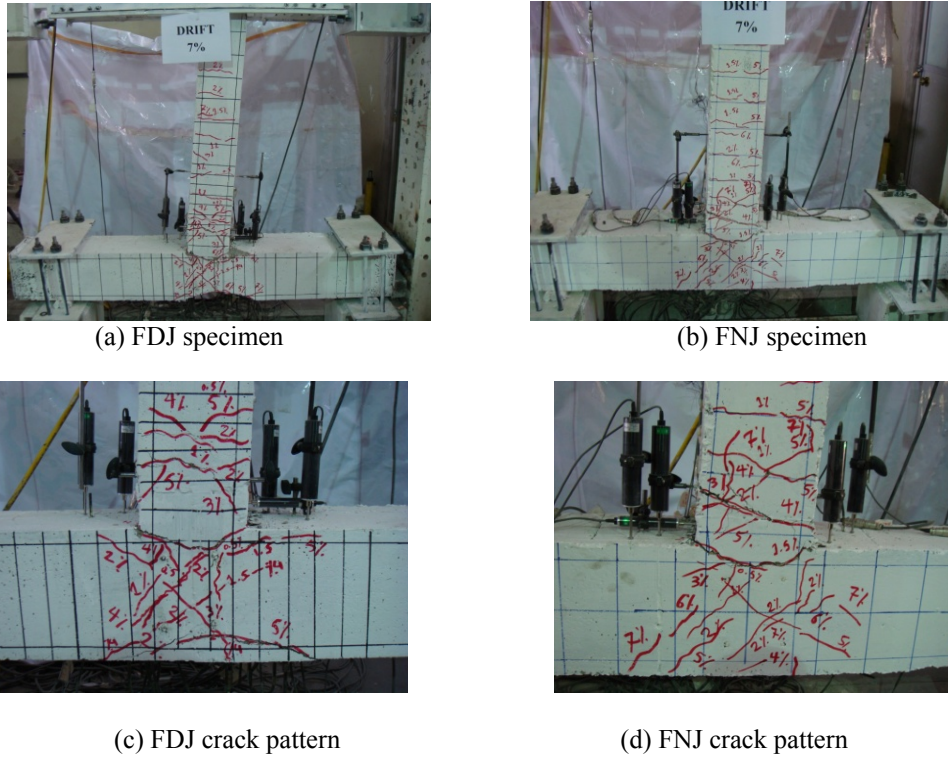


Fig. 6. Joint specimens at the end of loading

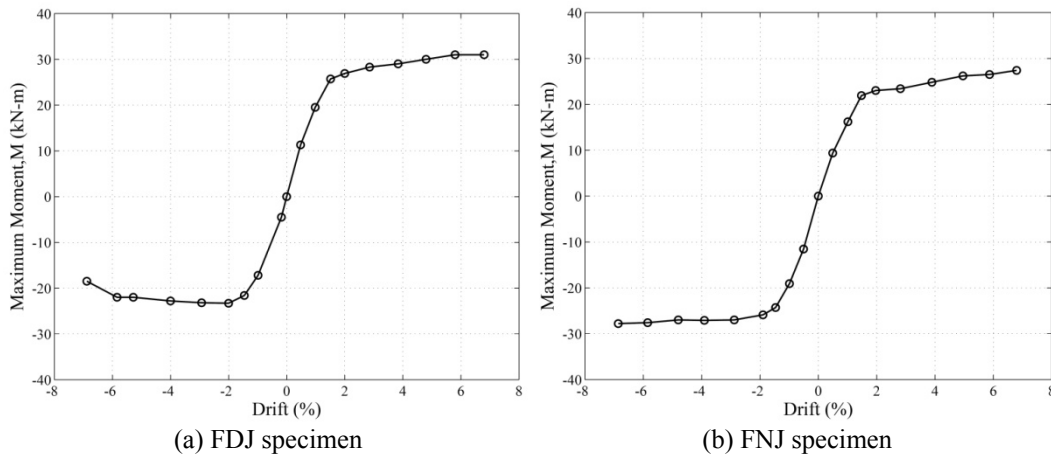


Fig. 7. Moment-drift back-bone curves for experimental specimens

**4. STRAINS IN JOINT STIRRUPS**

Positions of strain gauges instrumented on FRP stirrups and steel longitudinal reinforcements have been shown in Fig. 8. The first stirrup (at the distance of 50 mm from the column side) applied moment-strain diagram is shown in Fig. 9. FRP stirrups strains at the end of loading in FDJ and FNJ specimens approached up to 0.088% and 0.061%, respectively. FRP stirrups strain in the panel zone (inside of joint) has been shown in Fig. 10, maximum strain at the end of loading for FDJ and FNJ specimens were 0.24 and 0.6%, respectively. In Fig. 11, moment-strain diagram of 1st stirrup of column at a distance 50 mm from the column side was represented. At the end of loading, maximum strain of stirrups in FDJ and FNJ was 0.051 and 0.074%, respectively. Maximum strains of the first stirrup of beam and stirrups of inside joint at each specimen have been shown in Table 5.

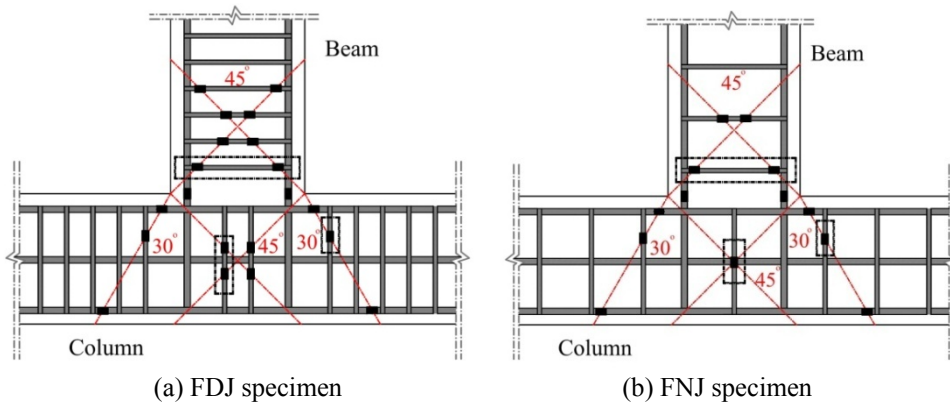


Fig. 8. Position of strain gauges on stirrups and longitudinal reinforcements,

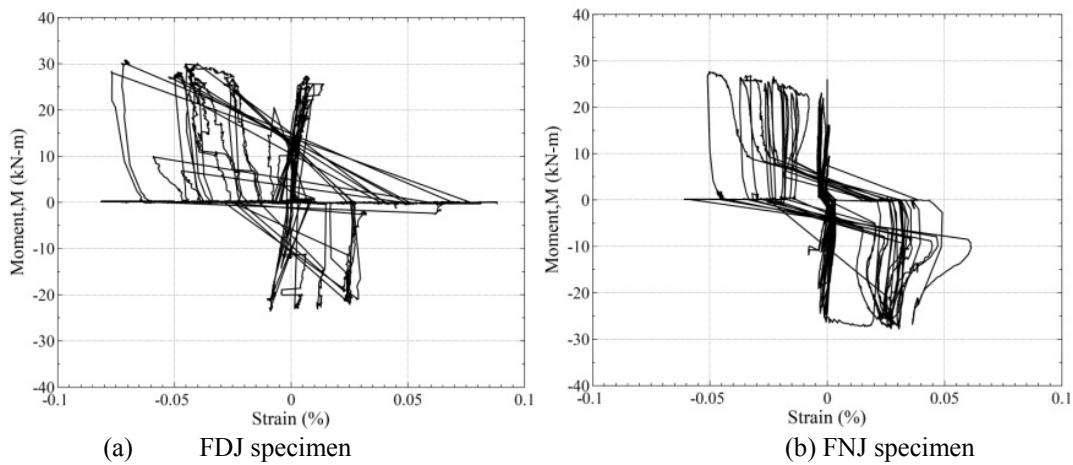


Fig. 9. Moment-strain diagram of the first stirrup in joint beam

Table 5. Maximum strains for first stirrup of beam and column and stirrup of joint source region

Specimen	Maximum strain of first stirrup of beam(%)	Maximum strain of joint region stirrup (%)	Maximum strain for first stirrup of column(%)
FDJ	0.088	0.24	0.051
FNJ	0.061	0.6	0.074

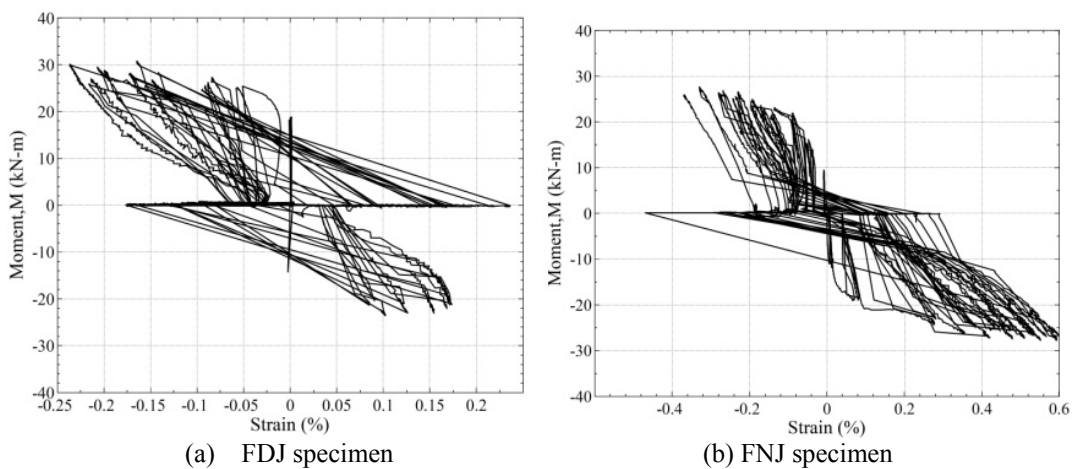


Fig. 10. Moment-strain diagram of stirrups in panel zone

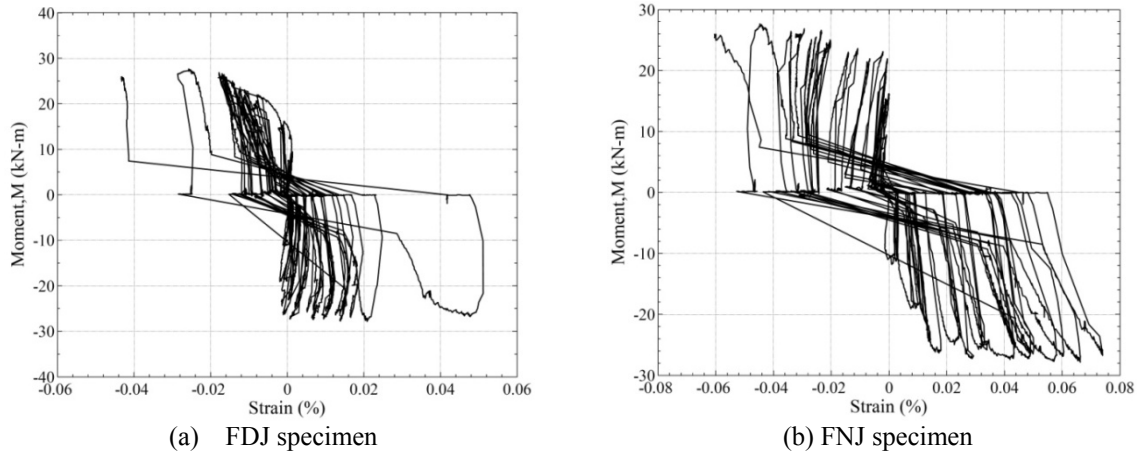


Fig. 11. Moment-strain diagram for 1<sup>st</sup> stirrup of column

### 5. FRP STIRRUPS EFFECTS ON MOMENT-CURVATURE AND ENERGY ABSORPTION

Moment-curvature diagram of a reinforced concrete section depicts its nonlinear bending characteristics exactly. In fact, this diagram shows the value of moment of a section regarding the initial state for a certain concrete section with definite distribution of longitudinal reinforcement, for a given axial force. Fig. 12 shows the moment-curvature diagram of beam (50 mm apart from column side). Maximum rotation of cross section for FDJ and FNJ is 0.058 and 0.057 radian, respectively. Energy absorption diagram of two specimens were presented in Fig. 13. Energy absorption diagram for joints can be obtained from the sum of the cross sections of hysteresis loops for drifts at loads not lower than 85% of maximum loading. According to this curve, both specimens absorbed the same low amount of energy up to 1.5% drift because of their initial crack patterns prior to the effectiveness of FRP stirrups. After 2% drift, the difference in energy absorption between FDJ and FNJ specimens was increased, so the value of energy absorption of ductile FDJ specimen was 3610 kN.m which was 1.18 times of maximum value corresponding to FNJ up to 7% drift. Stiffness variations diagram of joints against beam tip displacement is shown in Fig. 14, these diagrams are the same for both specimens.

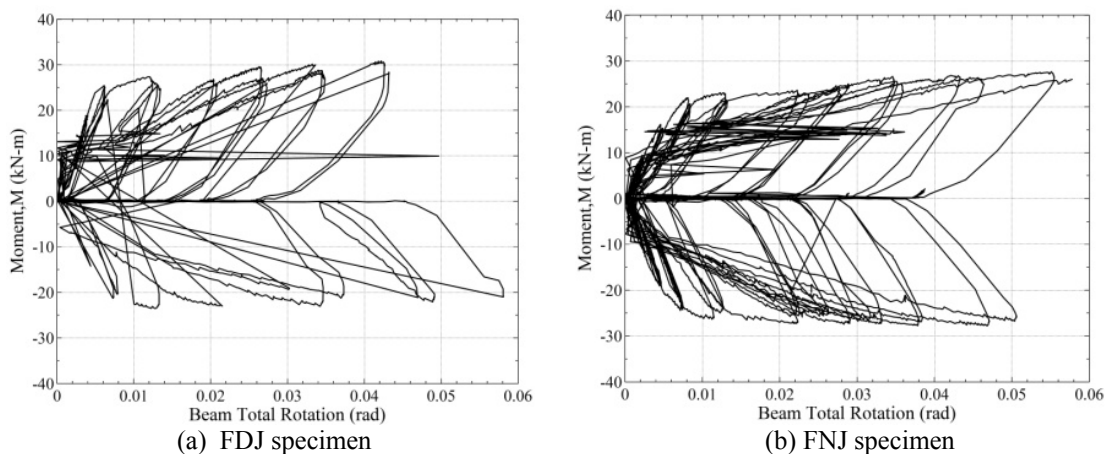


Fig. 12. Moment-curvature diagram for end of joints beam

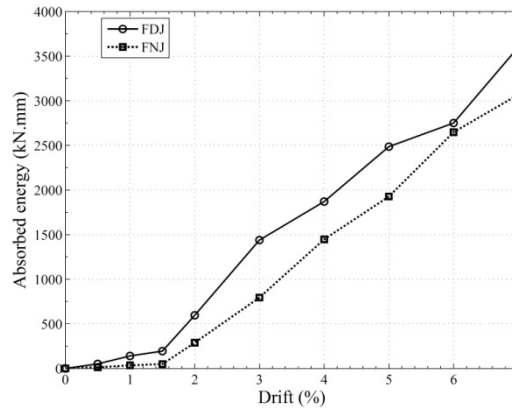


Fig. 13. Energy absorption diagram of the experimental specimens

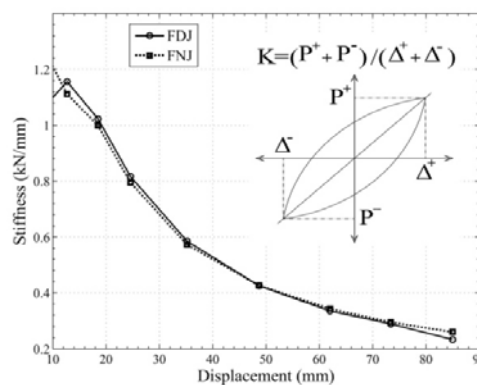


Fig. 14. Stiffness variation diagram of joints against displacement

### 6. FINITE ELEMENT ANALYSIS

Three types of elements (Solid65, Link8, Solid45) in Ansys program were adopted in the FE models of joint specimens. Solid65 element was defined by eight nodes, having three degrees of freedom at each node, widely used for 3-D modeling of solids with or without reinforcements. Link8 element is a uni-axial tension-compression element with three degrees of freedom at each node, namely translations in the nodal x, y, and z directions. It was used for modeling both longitudinal and transverse reinforcements in the concrete joints. The modeling of steel reinforcement was carried out using the discrete model in which rebar elements were connected to concrete mesh nodes. The layered Solid45 element was used for modeling the steel reaction plates [20]. The concrete behaves differently under different types and combinations of stress conditions due to the progressive micro cracking at the interface between the mortar and the aggregates (transition zone). The propagation of these cracks under the applied loads contributes to the nonlinear behavior of the concrete.

The mesh employed for the study had element length of 50 mm in beam and column of joint, whereas 20 by 50mm element size was used in the cover of joints. The h-method was used for analysis and this method requires a finer mesh. The ANSYS program will continue to do equilibrium iterations until the convergence criteria are satisfied. In this paper, L2-norm of displacement tolerance equal to 0.2% was used. It is appropriate for the analysis of all models. In most cases, an L2-norm check on displacement with tolerance equal to 0.2% is also used in addition to the displacement norm check. The program will check for displacement convergence by comparing the square root sum of the squares (SRSS) of the displacement imbalances against the product of VALUE\*TOLER (in this study=0.01). Concrete in

compression was considered to be linear-elastic up to about  $0.3f_c$ , where  $f_c$  was the cylinder compressive strength. The smeared crack plastic model used in the current study requires a biaxial state for concrete, for which the theoretical failure surface proposed by William-Warnke [21] was considered, as shown in Fig. 15-a. Moreover, the concrete uni-axial compression law was also necessary for simulation; therefore numerical expressions (Desayi and Krishnan [22]) were used to construct the uni-axial compressive stress-strain curve as shown in Fig. 15-b. In the William–Warnke concrete model,  $\sigma_{xp}$  and  $\sigma_{yp}$  are the most significant nonzero principal stresses in the x and y directions, respectively. In this smeared crack model, a smooth crack could close and all the material stiffness in the direction normal to the crack may be recovered.

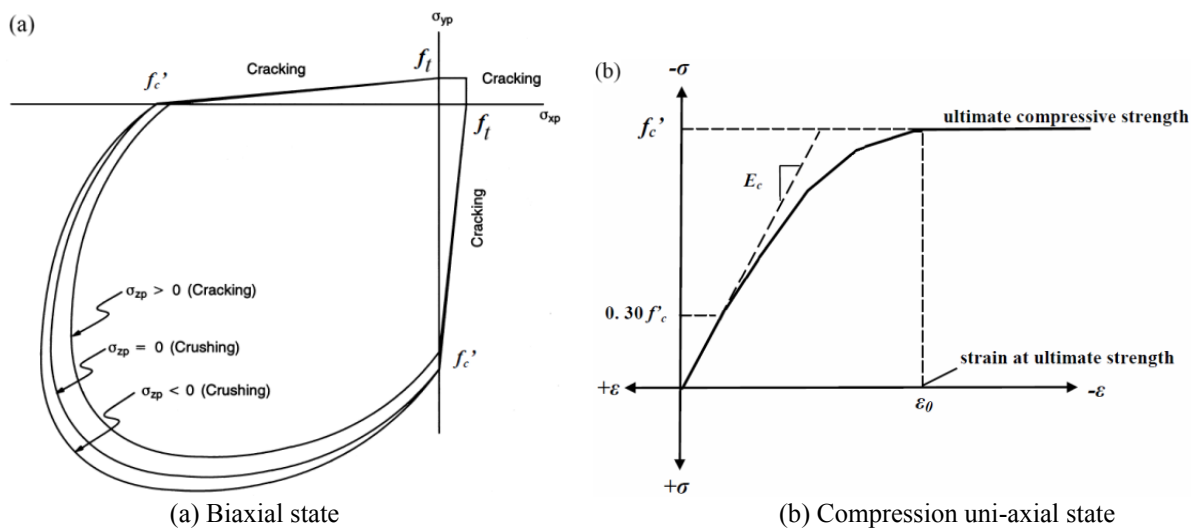


Fig. 15. Constitutive laws to concrete

The used material properties for the all concrete joint specimens have  $f_c' = 30MPa$ ,  $f_t = 4.1MPa$ ,  $E_c = 23GPa$ , and Poisson’s ratio  $\nu = 0.2$  conforming to the properties of experimental joint specimens. The kinematic hardening rule including Bauschinger effect and Von-Mises yield criteria was used for steel bars. In this study, Young’s modulus was  $E_s = 200,000MPa$ ,  $f_y = 260MPa$ , and Poisson’s ratio  $\nu = 0.3$ . Control of rupture in FRP strips is done through strain control. Using dimensions of experimental specimens, FE model of concrete beam is constructed and shown in Fig. 16. Moment-drift diagram of FE and experimental models is represented in Fig. 17, indicating a good agreement between FE and experimental model. Characteristics of experimental and FE models are provided in Table 6. There is a little difference between FE and the experimental models, the difference for displacement corresponding to first yielding of longitudinal bar, yielding of longitudinal reinforcements and ultimate loading were 6.7% , 3.6% 10.5%, respectively.

Table 6. Comparison of FE and experimental models

Specimen	$\Delta_y (mm)$	$M_y (kN.m)$	$\Delta_u (mm)$	$M_u (kN.m)$	Variation percent compared to experimental model			
					$\Delta_y \%$	$M_y (\%)$	$\Delta_u \%$	$M_u (\%)$
Experimental	9.89	15.26	85	31.25	6.7	5.2	3.6	10.5
FE	10.56	16.05	81.9	34.21				

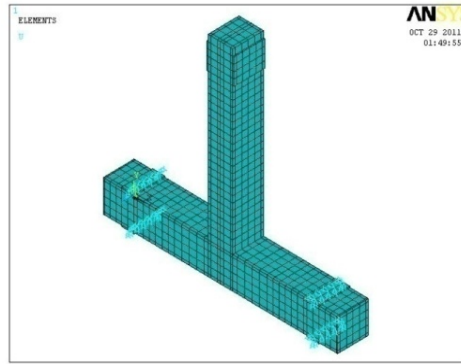


Fig. 16. FE Model of experimental FDJ specimens

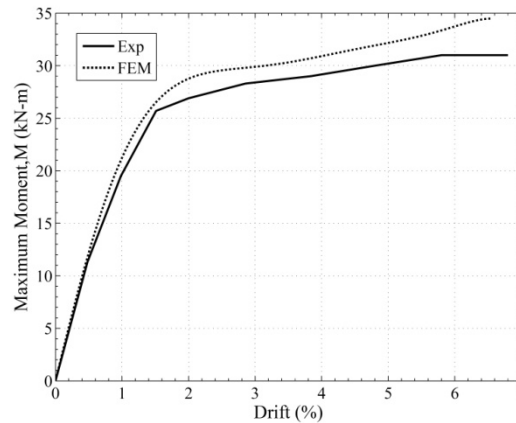


Fig. 17. Moment-drift diagram of FE and experimental models

**a) Finite element models of joints**

To assess the effects of FRP strips spacing on reinforced concrete joints, two groups of concrete joints with different dimensions and reinforcements were constructed. The first joint had ductile condition with closed space FRP stirrups and the second had non-ductile condition with wider spacing stirrups. FRP stirrups space in second specimen of each group was twice that of the first one. Numerical models had compressive strength of 30 MPa and steel longitudinal bars specifications the same as those at experimental ones. Selection of finite element specimen dimensions should satisfy the idea of weak beam-strong column. Dimensions and longitudinal reinforcement of modeled joints have been shown in Table 7. FRP stirrups cross sections have been presented in Table 8. FE models constructed by ANSYS software have been presented in Fig.18.

Table 7. Specification of FE modeled joints

Group No	Specimen name	Beam dimensions (mm)		Column dimensions (mm)		Reinforcement in top and down	Column reinforcement
		Height	Width	Height	Width		
1	J1D	400	500	500	500	4 $\phi$ 20	12 $\phi$ 20
	J1U	400	500	500	500	4 $\phi$ 20	12 $\phi$ 20
2	J2D	550	650	650	650	5 $\phi$ 25	16 $\phi$ 25
	J2U	550	650	650	650	5 $\phi$ 25	16 $\phi$ 25

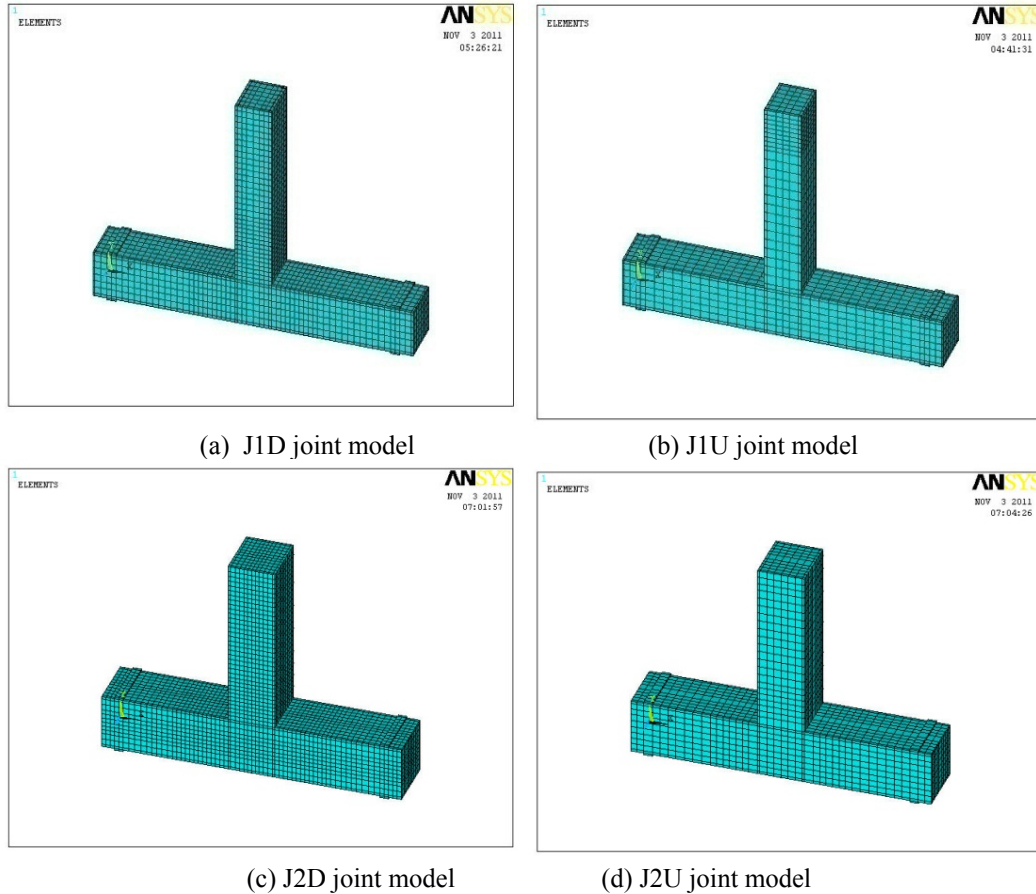


Fig. 18. Models constructed in ANSYS

Table 8. FE modeled FRP stirrups specification

Group No	Specimen name	Stirrups cross section ( $mm^2$ )	Stirrup space in ductile region (mm)	Stirrup space in non-ductile region (mm)
1	J1D	8	100	200
	J1U	8	200	200
2	J2D	10	150	300
	J2U	10	300	300

### b) Load-Displacement behavior of FE Specimens

Selected joints were subjected to the incremental loading at the end of the beam. Load-displacement diagrams of four specimens have been shown in Fig. 19. Loading of all specimens was applied up to 7% drift equal to 140 mm displacement. According to analysis carried out on both groups, joint with FRP ductile stirrups had higher loading capacity compared to joints with non-ductile FRP stirrups. In both groups, up to displacement of 7 mm, load-displacement diagrams were the same. From 7 to 40 mm displacement, difference between load-displacement diagrams was relatively increased. From 50 to 140 mm, the difference between both groups' diagrams was increased up to 8.7% and 7.5 % at the first J1D specimen and the second J2D higher than forces corresponding to J2U specimen, respectively. FE analysis results of the specimen are represented in Table 9. According to the obtained results, the displacement in which the first yield of longitudinal reinforcement is observed was decreased 15% compared to J1U, but the 19% decrease happened in the second group of J2D specimens compared to J2U specimens. In both groups, the first joint of each group (J1D and J2D) with ductile conditions has the higher ductility

coefficient compared to non-ductile joints (J1U and J2U). Ductility coefficient for J1D joint was 8.69, which was 11.5% higher than the J1U specimens. Moreover, in the second group, J2D joint has ductility coefficient of 8.09, which is 22% higher than J2U specimens.

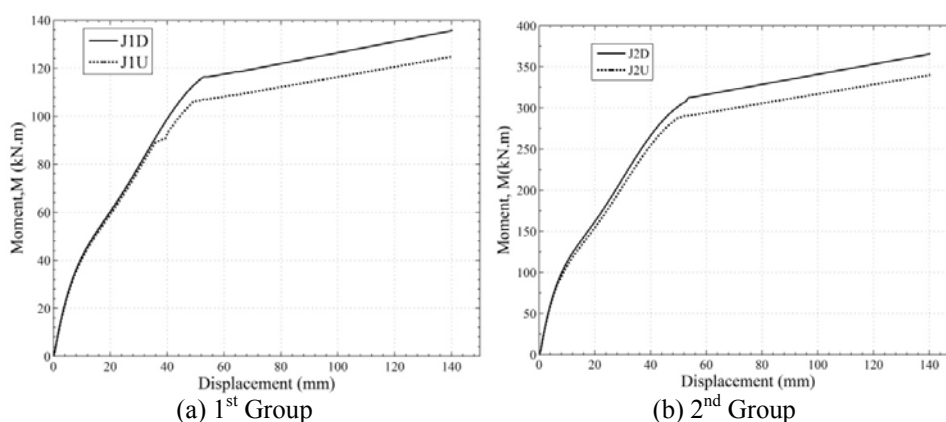


Fig. 19. Diagram of force-displacement of two joint groups

Table 9. Yield and ultimate load, displacement and ductility coefficient of FE models

Specimen	$\Delta_y (mm)$	$M_y (kN.m)$	$\Delta_u (mm)$	$M_u (kN.m)$	$\mu = \frac{\Delta_u}{\Delta_y}$
J1D	16.1	57.15	140	135.6	8.69
J1U	19.05	65.6	140	123.9	7.35
J2D	17.3	138.7	140	365.3	8.09
J2U	21.23	142.2	140	338.6	6.59

## 7. CONCLUSION

Experimental and finite element investigations were studied here to assess the effects of CFRP stirrup spacing on the cyclic behavior of concrete joints. Two concrete joints with the same characteristics reinforced with longitudinal steel bars and transverse CFRP stirrups at the different spaces were experimentally constructed and tested, then the numerical models were validated and new models were produced. According to the behavioral observations and obtained results of experimental cyclic loading of two reinforced concrete beam-column joints and numerical models, the following results were drawn:

- Both experimental specimens with FRP closed ductile stirrup (designed based on seismic provision codes) and non-ductile specimen with wider spacing FRP stirrup showed stable behaviors without significant strength degradation.
- Maximum strain of FRP tested ductile and non-ductile joints were 0.24% and 0.6% and the maximum strain experienced by joint source stirrup was close to the allowable design code, showing the effectiveness of these stirrups on the increasing ductility. Therefore the ductile FRP joints showed 26% higher ductility coefficients and 18% higher energy absorption than those of non-ductile joints, even though their capacity difference was only 12%. Test results indicated that the FRP closed spacing stirrups equal to a quarter of the effective depth of the beam had an extra FRP stirrup inside of the joint, and had a significant effect on increasing ductility of seismic designed joints, however, little effect on increasing the capacity.

Numerical analysis showed that all specimens reinforced with FRP stirrups designed based on Design code ductility regulations at closed space had an average 8% higher loading capacity and FE modeled joints with closed ductile stirrups condition had higher ductility coefficients up to 20% compared to wide stirrup spacing joints.

**Acknowledgment:** This research was financially supported by research bureau of Semnan University. The authors' would like to thank the university and also the staff who provided technical support, especially the structural lab Technician Mr. Bakhshae.

## REFERENCES

1. Fukuyama, H. & Masuda, Y. (1995). *Structural performances of concrete frame reinforced with FRP reinforcement, non-steel (FRP) reinforcement for concrete structures*. Edited by Taerwe. E&FN Spon, London, pp. 275-286.
2. Sharbatdar, M. K. (2003). Concrete columns and beams reinforced with FRP bars and grids under monotonic and reversed cyclic loading. Ph.D. Thesis, University of Ottawa, Ottawa, Canada.
3. Kheyroddin, A., Naderpour, H., Ghodrati Amiri, G. & Hoseini Vaez, S. R. (2011). Influence of carbon fiber reinforced polymers on upgrading shear behavior of RC coupling beams. *Iranian Journal of Science & Technology, Transactions of Civil Engineering*, Vol. 35, No. C2.
4. Ceroni, F. (2010). Experimental performances of RC beams strengthened with FRP materials. *Journal of Construction and Building Materials*, Vol. 24, pp. 1547–1559.
5. Sharbatdar, M. K., Saatcioglu, M. & Benmokrane, B. (2011). Experimental investigation behaviour of concrete connections reinforced with CFRP bars & grids. *Composite Structures*, Vol. 93, Issue 10, pp. 2439-2449.
6. Mostofinejad, D. & Talaeitaba, S. B. (2006). Finite element modeling of RC connections strengthened with FRP laminates. *Iranian Journal of Science & Technology, Transaction B, Engineering*, Vol. 30, Issue B1, pp. 21-30.
7. ACE Consulting Engineers, Brisbane, Australia. (2010). Strength and ductility of FRP web-bonded RC beams for the assessment of retrofitted beam–column joints. *Journal of Composite Structures*, Vol. 92.
8. ACI Committee 440. (2001). Guide for the design and construction of concrete reinforced with FRP bars. ACI440.1R-03, American Concrete Institute, USA.
9. Canadian Standards Association, S806-02. (2002). Design and construction of building components with fiber-reinforced polymers. CSA, Rexdale Ontario.
10. Japanese Society of Civil Engineers (JSCE). (1997). Recommendation for design and construction of concrete structures using continuous fiber reinforcing materials. *Concrete Engineering Series*, Vol. 23. Tokyo.
11. Eshghi, S. & Zanjanizadeh, V. (2008). Retrofit of slender square reinforced concrete columns with glass fiber-reinforced polymer for seismic resistance. *Iranian Journal of Science & Technology, Transaction B, Engineering*, Vol. 32, Issue B5, pp. 437-450 .
12. Berg, A. C., Bank, L. C., Oliva, M. G. & Russell, J. S. (2006). Construction and cost analysis of an FRP reinforced concrete bridge deck. *Construction and Building Materials*, Vol. 20, pp. 515–526.
13. Nanni, A., Okamoto, T., Tanigaki, M. & Osakada, S. (1993). Tensile properties of braided FRP rods for concrete reinforcement. *Cement and Concrete Composites*, Vol. 15, pp. 121-129.
14. Li, J., Bakoss, S., Samali, B. & Ye, L. (1999). Reinforcement of concrete beam–column connections with hybrid FRP sheet. *Composite Structures*, Vol. 47, Issues 1–4, pp. 805-812.
15. Gadve, S., Mukherjee, A. & Malhotra, S. N. (2009). Corrosion of steel reinforcements embedded in FRP wrapped concrete. *Construction and Building Materials*, Vol. 23, pp. 153-161.
16. Lau, D. & Pam, H. (2010). Experimental study of hybrid FRP reinforced concrete beams. *Engineering Structures*, Vol. 32, Issue 12, pp. 3857-3865.
17. Gravina, R. J. & Smith, S. T. (2008). Flexural behaviour of indeterminate concrete beams reinforced with FRP bars. *Engineering Structures*, Vol. 30, Issue 9, pp. 2370-2380.
18. ACI Committee 318 (2005). *Building code requirements for reinforced concrete (ACI 318-05)*. American Concrete Institute, Farmington Hills, MI.

19. Sharbatdar, M. K., Kheyroddin, A. & Emami, E. (2012). Cyclic performance of retrofitted reinforced concrete beam–column joints using steel prop, *Journal of Construction and Building Materials*, Vol. 36, pp. 287–294).
20. ANSYS User's Manual Version 10.0. (2006). Houston: Swanson Analysis Systems Inc.
21. Willam, K. J. & Warnke, E. P. (1975). Constitutive model for the triaxial behavior of concrete. *Proceedings of International Association for Bridge and Structural Engineering*. Bergamo (Italy): ISMES.
22. Desayi, P. & Krishnan, S. (1964). Equation for the stress-strain curve of concrete. *Journal of the American Concrete Institute*, Vol. 61, pp. 345-350, March.